Article

Not peer-reviewed version

Actinide ion (Americium-241 and Uranium-232) Interaction with Hybrid Silica-Hyperbranched Poly(ethylene imine) Nanoparticles and Xerogels

Ioannis Ioannidis , Ioannis Pashalidis * , Michael Arkas *

Posted Date: 9 August 2023

doi: 10.20944/preprints202308.0614.v1

Keywords: Am-241 and U-232; dendritic polymers; silica xerogels; composites; dendrimers; water purification; radioactive wastewater; radionuclide removal; thermodynamic; environmental remediation; water decontamination

Article

Actinide Ion (Americium-241 and Uranium-232) Interaction with Hybrid Silica-Hyperbranched Poly(ethylene imine) Nanoparticles and Xerogels

Ioannis Ioannidis [1], Ioannis Pashalidis [1,*] and Michael Arkas [2,*]

[1] Laboratory of Radioanalytical and Environmental Chemistry, Department of Chemistry, University of Cyprus, P.O. Box 20537, Cy-1678 Nicosia, Cyprus; ioannides.c.ioannis@ucy.ac.cy (I.I.)
[2] National Centre for Scientific Research "Demokritos", Institute of Nanoscience and Nanotechnology, Athens, Greece;
* Correspondence: m.arkas@inn.demokritos.gr (M.A.); paschalidis.ioannis@ucy.ac.cy (I.P.);

Abstract: The binding of actinide ions (Am(III) and U(VI)) in aqueous solutions by hybrid silica-hyperbranched poly(ethylene imine) nanoparticles (NP) and xerogels (XG) has been studied by means of batch experiments at different pH values (4, 7 and 9) under ambient atmospheric conditions. Both materials present relatively high removal efficiency at pH 4 and pH 7 (> 70%) for Am(III) and U(VI). The lower removal efficiency for the nanoparticles is basically associated with the compact structure of the nanoparticles and the lower permeability and access to active amine groups compared to xerogels, and the negative charge of the radionuclide species formed under alkaline conditions (e.g. $UO_2(CO_3)_3^{4-}$ and $Am(CO_3)_2^-$). Generally, the adsorption process is relatively slow due to the very low radionuclide concentrations used in the study and is basically governed by the actinide diffusion from the aqueous phase to the solid surface. On the other hand, the adsorption is favored with increasing temperature assuming that the reaction is endothermic and entropy-driven, which is associated with increasing randomness at the solid-liquid interphase upon actinide adsorption. To the best of our knowledge, this is the first study on hybrid silica-hyperbranched poly(ethylene imine) nanoparticle and xerogel materials used as adsorbents for americium and uranium at ultra-trace levels. Compared to other adsorbent materials used for binding americium and uranium ions, both materials show far higher binding efficiency. Xerogels could remove both actinides even from seawater by almost 90%, whereas nanoparticles could remove uranium by 80% and americium by 70%. The above, along with their simple derivatization to increase the selectivity towards a specific radionuclide and their easy processing to be included in separation technologies, could make these materials attractive candidates for the treatment of radionuclide/actinide contaminated water.

Keywords: Am-241 and U-232; dendritic polymers; silica xerogels; composites; dendrimers; water purification; radioactive wastewater; radionuclide removal; thermodynamic; environmental remediation; water decontamination

1. Introduction

Americium (Am) and uranium (U) are two elements belonging to the actinide series [1]. These elements exhibit different species when subjected to different pH environments and oxidation states. In aqueous solutions, uranium forms various hydrolysis and carbonate complexes, such as UO_2^{2+} in acidic conditions, $UO_2(OH)_2$ and UO_2OH^+ near neutral pH, and $UO_2(CO_3)_2^{2-}$, $UO_2(CO_3)_3^{4-}$ in alkaline environments [2,3]. On the other hand, for americium, Am^{3+} dominates in acidic aqueous solutions and under normal conditions, and Am(III)-hydroxycarbonate ($Am(CO_3)(OH)$) shows limited solubility and $Am(CO_3)_3^{3-}$ is the dominant species in alkaline aqueous environment [4,5]. In the literature, there are only a few studies that report on the adsorption of these two radionuclides by various adsorbent materials such as microplastics [6] and aerogels [7]. According to those studies, the adsorption mechanism seems to depend on both the radionuclide speciation and the surface-active sites, including charge/polarization and complex formation properties.

 doi:10.20944/preprints202308.0614.v1

Due to the severity of the continuously increasing accumulation of these radioactive ions in aquatic media, there has been extensive research on appropriate methods such as cation exchange, precipitation, and extraction to address the problem. Adsorption though is established as the most effective. The incorporation of radionuclides into the substrates proceeds mainly via two mechanisms: 1) electrostatic attraction between the solubilized ion forms and oppositely charged adsorbents producing outer sphere complexes or 2) formation of coordination compounds with the terminal functional groups of the adsorbents (e.g., -COOH, -NH_2, -OH) yielding inner-sphere complexes [8–12]. Effective and specific pollutant retention materials were discovered to demonstrate extraordinary properties. More specifically from a purely organic point of view microplastics [13], biopolymers [14], and conventional polymers [15,16] are the more promising representatives while distinguished classes of inorganic compounds include metal oxides [17], minerals [18], carbon allotropes [19]. The combination of organic and inorganic moieties expectedly yields a wider variety of prominent adsorbents for instance metal-organic frameworks (MOFs) [20–22] aerogels [23–26], organic-inorganic composites [27,29], and hybrids [30,31].

The applicability of dendritic polymers [32–34] in water purification is nowadays well-established [35,36]. This fourth class of macromolecular architecture is generated by the replacement of the typical linear polymerization, branching, or crosslinking with radial propagation of the monomeric units [37]. Because of their noteworthy branched architecture, reminiscent of the tree-like structures commonly encountered in nature (roots and branches of trees, arteries, river deltas [38] they may adapt to almost all conventional pollutant removal methods. For this reason, there is a rich literature on adsorption [39] catalytic degradation [40], and ultrafiltration [41] procedures. The efficacity of all main dendritic classes relies on the three main structural components that define their architecture. a) The core or focal point in the case of dendrons. b) The internal containing cavities formed by the polymerized units: the "branches" of the "tree. They define the adsorption properties of the whole molecule and may be modified accordingly to incorporate the majority of pollutants. c) The peripheral groups that may undergo functionalization to fine-tune solubility, electrostatic interactions, and any other desired property.

Since adsorption proved the more prosperous method for aquatic systems remediation from industrial radioactivity pollution, research on the performance of dendritic polymers in this particular domain attracted analogous interest that led to the development of specialized solutions [42–45]. To extend the proof of concept to an economically feasible implementation the first requirement is diminishing the cost of the dendritic polymer. An obvious approach is to replace the expensive dendrimers [46–50] with their non-symmetric counterparts, hyperbranched polymers [51–57]. Their properties and overall behavior are similar and they have already taken the place of their monodisperse counterparts in many implementations in diagnostics [58–60], biosensors [61,62], antimicrobial protection [63], liquid crystals [64–66] and drug delivery [67].

A second necessity is a supporting substrate that protects the organic moieties from chemical degradation and preferably also possesses pollutant retention capacity or other separation capabilities such as magnetic susceptibility. The combination with porous inorganic materials [68] is the most obvious formulation. There are three main approaches in this direction. a) Simple impregnation of the carrier with a solution of the hyperbranched polymer [69]. b) Chemical grafting of the dendritic polymer to the substrate [70,71]. c) immobilization of a functionalized derivative by polymerization into the pores of the supporting scaffold [72].

A fourth perspective that addresses both ecological and economic issues is based on the ability of hyperbranched poly(ethylene imine) (PEI) to mimic the action of silaffins and produce silica nanospheres [73]. Alternatively, the same molecules may intervene in the hydrogen bond network that forms during the gelation of orthosilicic acid and thus produce xerogels after drying. Both silica-PEI composites exhibited potent adsorbing capability for many aqueous pollutants [74,75]. The two synthesis procedures are very simple and take place at room temperature with no involvement of toxic organic solvents or byproducts. The present work aims to test these two species (nanospheres and xerogels) radionuclide adsorption kinetics and thermodynamics. The binding efficiency has been evaluated in terms of the linear adsorption constant K_d and the relative removal efficiency. The study

Preprints (www.preprints.org) | NOT PEER-REVIEWED | Posted: 9 August 2023 doi:10.20944/preprints202308.0614.v1

will be performed for factors such as pH and temperature for ultra-trace level as well as in seawater to define the optimal uranium and americium removal conditions.

2. Results and Discussion

2.1. Xerogel and Nanoparticle Characteristics

As established in the experimental section the two different forms of hybrid silica-PEI composites arise by modification of the orthosilicic acid/hyperbranched PEI ratio. The most profound difference thus is the dendritic polymer content of the nanoparticles which is more than double that of the xerogel [75]. The higher number of amino groups has a secondary consequence. The external charge of the adsorbents at pH 3 is similar. Their behavior though by increasing pH is completely disparate. The nanoparticles remain positive even at pH 9 albeit of a much lesser charge. In contrast, an abrupt reverse is observed for the xerogels that became negative even at pH 4 (Figure 1).

Besides the composition, the role of hyperbranched PEI is different in the creation of the final hybrid material. In the case of nanoparticles, the dendritic polymer functions as a catalyst and matrix and is positioned in the core of the composite enveloped by a shell of the produced silica. In the case of gels, there are no indications that PEI promotes gelation. Xerogel conformation has much lower anisotropy and consists both in the interior and the exterior of "islands" of dendritic polymers surrounded by a "sea" of siloxane and silanol groups. In this way, the cavities of the adsorbing polymer are more exposed to the radionuclides. Another significant variance is the pore structure. The xerogels have larger BET surfaces and much bigger pores [75]. The most important advantage of the xerogels though is their capability to be readily formed in restricted media for instance the pores of a ceramic support by simple immersion of the latter into a precursor gel solution. Thus, in addition to the classical powder formulation that may be dispersed into the contaminated water, there is also the option of coatings applied to continuous filtration filters. Their stability will be secured due to the *in-situ* polymerization.

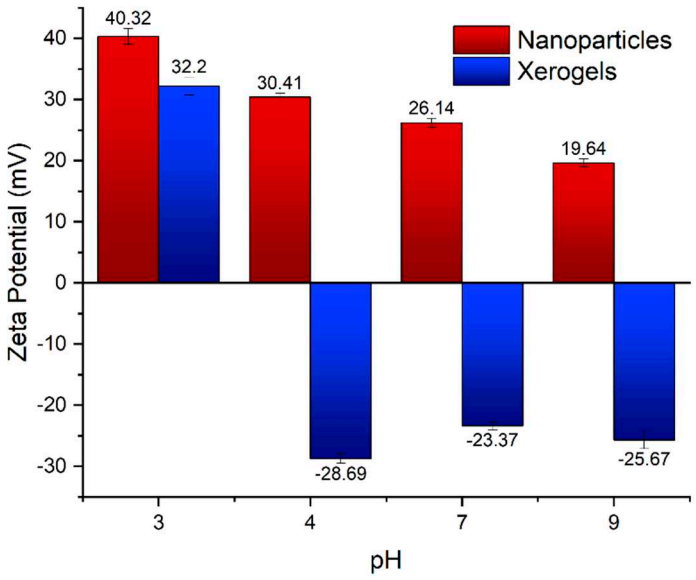

Figure 1. Surface charge of nanoparticles and xerogels in different pH.

Based on the above the binding of the actinides by the nanoparticles and xerogels is expected to occur via cation exchange between protons and the U(VI) or Am(III) cations and inner-sphere complex formation between the actinide cations and the polyimine moieties. In the case of uranium (e.g. uranyl moiety) interaction of the uranyl oxygens and ammonium protons is also possible favoring surface binding of U(VI) (Figure 2) [6,7].

Preprints (www.preprints.org) | NOT PEER-REVIEWED | Posted: 9 August 2023 doi:10.20944/preprints202308.0614.v1

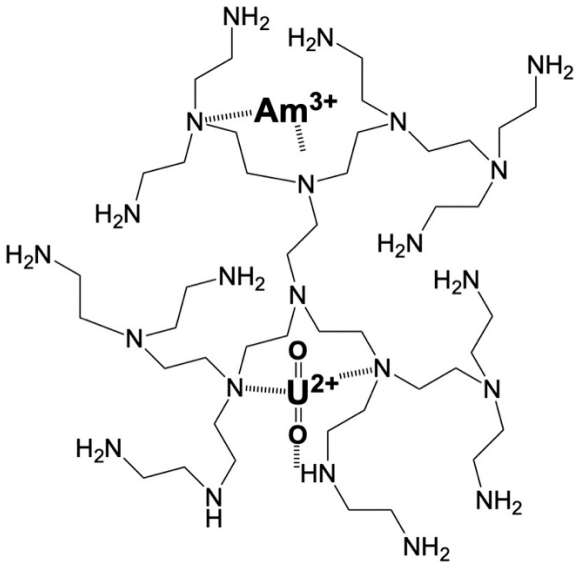

Figure 2. Schematic illustration of possible interactions of the actinide ions (Am^{3+} and UO_2^{2+}) with the PEI-based adsorbents.

2.2. Adsorption Kinetics

The time evolution of the relative actinide ion binding at pH 4, pH 7, and pH 9 is graphically presented in Figures 3a, 3b, and 3c. It is clear that the adsorption kinetics differ significantly between the different adsorbents (e.g. nanoparticles and xerogels) and actinide ions (e.g. U(VI) and Am(III)), and that pH plays a main role since it determines both the charge of the surface and the actinide speciation in solution. According to the kinetic data, which have been obtained for the adsorption of uranium and americium by the nanoparticle and xerogel adsorbents at three different pH regions, generally, uranium presents higher adsorption rates compared to americium. Regarding the adsorbents, under acidic conditions (pH 4) the nanoparticles present higher adsorption kinetics for both radionuclides, whereas at pH 9 the xerogels show higher adsorption kinetics than the nanoparticles. Under neutral conditions, the adsorption kinetics are almost similar, except for the adsorption of americium by the nanoparticles, which present lower adsorption kinetics. Moreover, the experimental kinetic data are well described by the *Lagergren* equation (e.g. the pseudo-first-order kinetic model), indicating that the binding rate is dependent only on the actinide concentration, which is expected for systems performed at ultra-trace levels [76,77]. Following, the thermodynamic experiments were evaluated after 10 days of contact time in order to assure equilibrium conditions.

Preprints (www.preprints.org) | NOT PEER-REVIEWED | Posted: 9 August 2023 doi:10.20944/preprints202308.0614.v1

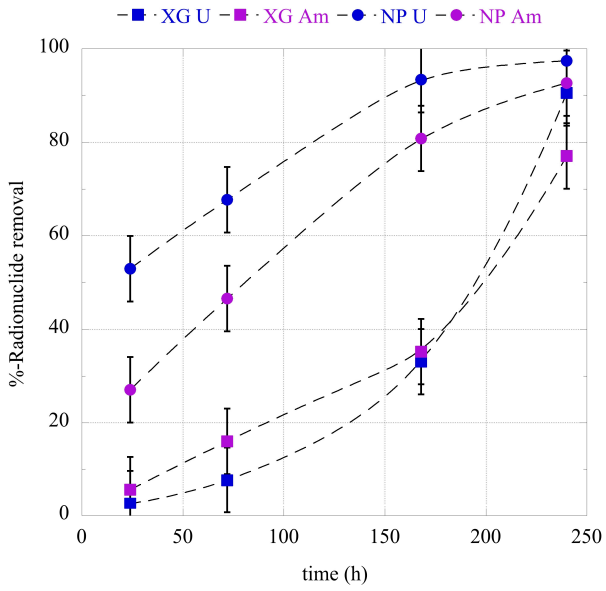

a)

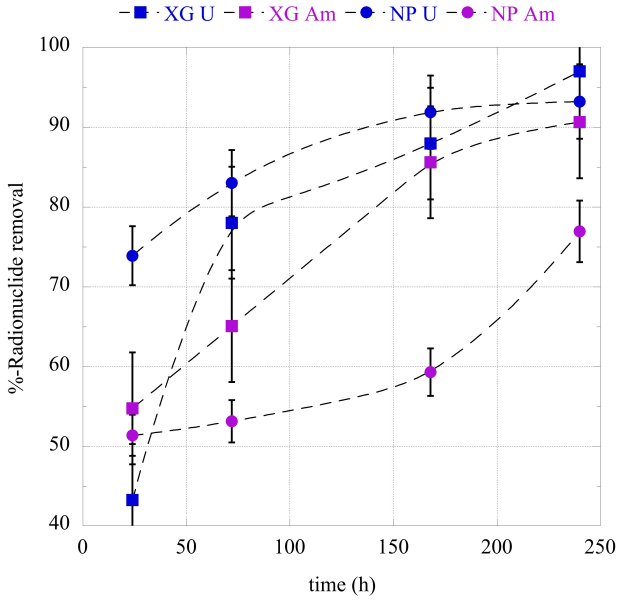

b)

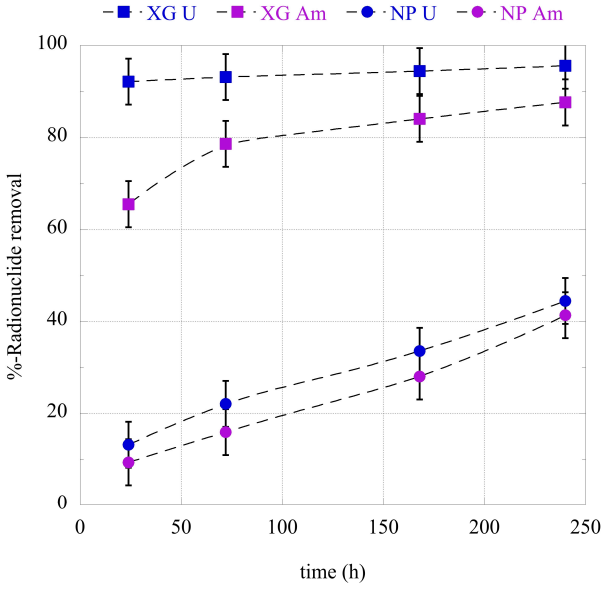

c)

Preprints (www.preprints.org) | NOT PEER-REVIEWED | Posted: 9 August 2023 doi:10.20944/preprints202308.0614.v1

Figure 3. U(VI) and Am(III) adsorption kinetics by the PEI nanoparticles (NP) and xerogels (XG) at ultra-trace levels at a) pH 4, b) pH 7, and c) pH 9. Experimental conditions: 0.5 Bq/mL U-232 and Am-241 in 10 mL total volume and ambient conditions.

2.3. pH effect on the actinide binding efficiency

The %-relative actinide ion removal by the nanoparticle and xerogel adsorbents is graphically presented in Figure 4 and indicates that in the case of xerogels, the pH does not significantly affect the removal efficiency. On the other hand, the nanoparticle affinity towards both radionuclides is considerably affected by pH. Specifically, the %relative removal decreases with increasing pH and at pH 9 the values of the relative removal are below 50%. To understand this behavior, we must take into account the predominant radionuclide species at each pH and their charges in conjunction with those of the adsorbents [7]. At low pHs, the predominant ion species (Am^{3+}, UO_2^{2+}) are positively charged and electrostatically rappelled by the homonymous charges of both adsorbents. Yet their removal from the aqueous solution proceeds smoothly and is almost complete in the case of nanoparticles that exhibit a higher positive charge. This is a strong indication that adsorption proceeds mainly via the chelation mechanism affording inner-sphere complexes. At neutral pH the americium ions are positive (Am^{3+}, $AmCO_3^+$) justifying a small improvement in their incorporation into the negatively charged hydrogels. Uranium counterparts are neutral (UO_2CO_3) or positive (UO_2OH^+) and a possible explanation for the slight drop in the adsorption must be sought to the larger ion sizes and the core-shell structure of the nanoparticles. It seems that the bigger species are struggling to pass through the porous silica entourage to form coordination compounds with the hyperbranched PEI core. This effect becomes more intense in basic solutions where the negatively charged and much bulkier actinide species ($UO_2(CO_3)_3^{4-}$, $Am(CO_3)_2^-$ present a slightly lower affinity to the homonymous xerogels by repelling one another and experience a far greater steric hindrance when crossing the silica periphery of the nanoparticles resulting in considerably lower removal efficiency. Moreover, the data indicate that both materials present a higher affinity for U(VI) compared to Am(III). Compared to alginate aerogels the xerogels present significantly higher removal efficiency for both uranium and americium [7]. Similarly, the nanoparticles show higher relative removal efficiencies, except for pH 9, where the relative removal declines to values below 50%.

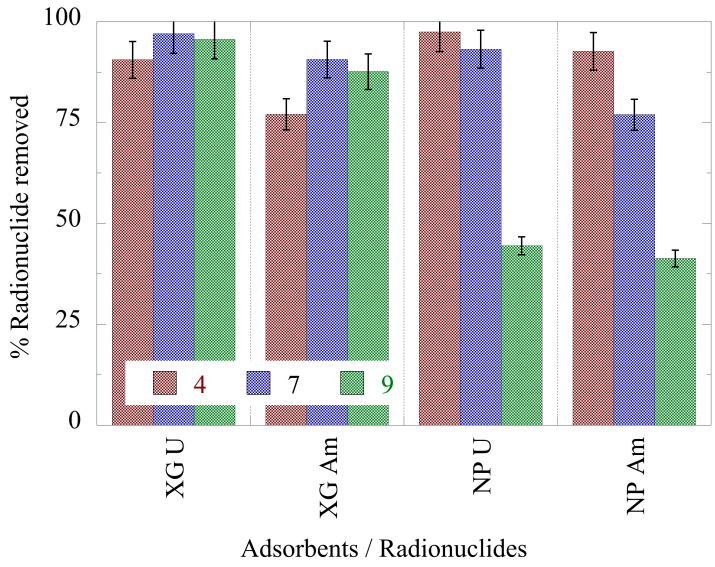

Figure 4. %-relative actinide ion removal by nanoparticles (NP) and xerogels (XG) at ultra-trace levels as a function of pH from aqueous solutions. Experimental conditions: 10 mL of the solution, with 0.5 Bq/mL for both U-232 and Am-241 tracers, in different pH (pH = 4, 7, 9) and at room temperature.

Preprints (www.preprints.org) | NOT PEER-REVIEWED | Posted: 9 August 2023 doi:10.20944/preprints202308.0614.v1

Regarding the K_d values (Figure 5), the highest values have been determined for the U(VI) adsorption by XG, which reaches a maximum value in neutral solutions. This behavior is attributed to the competitive reaction of protons in the acidic pH region, which occupy binding sites on the composite surface and the $UO_2(CO_3)_3^{4-}$ species, the formation of which is favored in the alkaline pH region (pH 9) stabilizing U(VI) in solution [78]. On the other hand, for the nanoparticles, that present generally lower K_d values, the maximum K_d value is observed in the weak acidic pH region (pH 4) and drops dramatically with increasing pH. Regarding Am(III), the associated K_d values present similar behavior with the corresponding K_d values of U(VI). However, the associated values K_d values of Am(III) are significantly lower than the corresponding K_d values of U(VI). The higher affinity of the xerogels and nanoparticles for U(VI) is of particular interest regarding uranium separation from trivalent actinide- and lanthanide-containing solutions. However, the associated K_d values are orders of magnitude lower indicating lower chemical affinity of the xerogels and nanoparticles for the studied actinides compared to the alginate aerogels. This could be associated with the lower density of the alginate aerogels but also with the fact that the PEI xerogels and nanoparticles have a larger number of binding sites available for actinide ion complexation compared to the alginate aerogels.

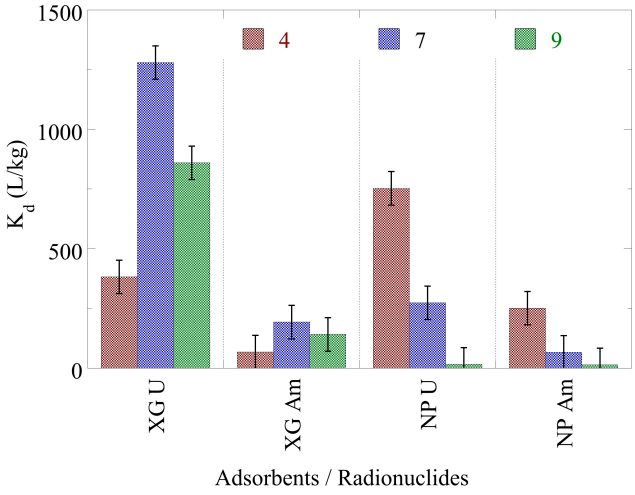

Figure 5. Adsorption efficiency ($\log_{10}K_d$) of U(VI) and Am(III) by nanoparticles (NP) and xerogels (XG) at ultra-trace levels as a function of pH from aqueous solutions. Experimental conditions: 10 mL of the solution, with 0.5 Bq/mL for both U-232 and Am-241 tracers, in different pH (pH = 4, 7, 9) and at room temperature.

2.4. Adsorption Thermodynamics

The temperature effect on the relative actinide ion removal is shown in Figures 6 and 7 for uranium and americium, respectively. The temperature increase from 25 °C to 35 °C, generally results in an increase in the removal efficiency indicating that the binding is favored with increasing temperature and that the entropy governs the adsorption process. However, at 45 °C the removal efficiency declines significantly due to changes in the structure of the adsorbents, which is associated with solvent molecule release at the given temperature. A similar effect was observed also in a previous study investigating the U(VI) adsorption by the same type of adsorbents at increased uranium concentrations [75].

Preprints (www.preprints.org) | NOT PEER-REVIEWED | Posted: 9 August 2023 doi:10.20944/preprints202308.0614.v1

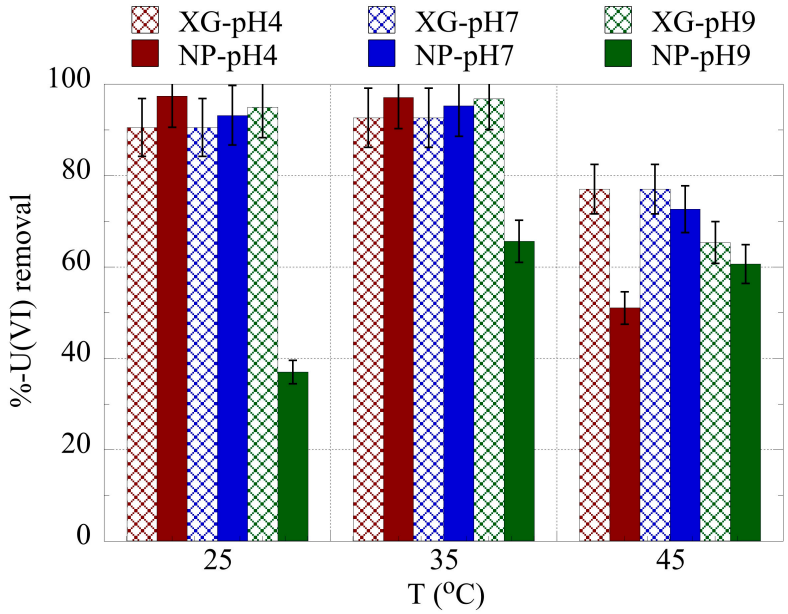

Figure 6. %-relative removal of U(VI) by nanoparticles (NP) and xerogels (XG) at ultra-trace levels as a function of pH and temperature. Experimental conditions: 10 mL of the solution, with 0.5 Bq/mL for both U-232 and Am-241 tracers, in different pH (pH = 4, 7, 9) and temperatures (25, 35, 45 ^{0}C).

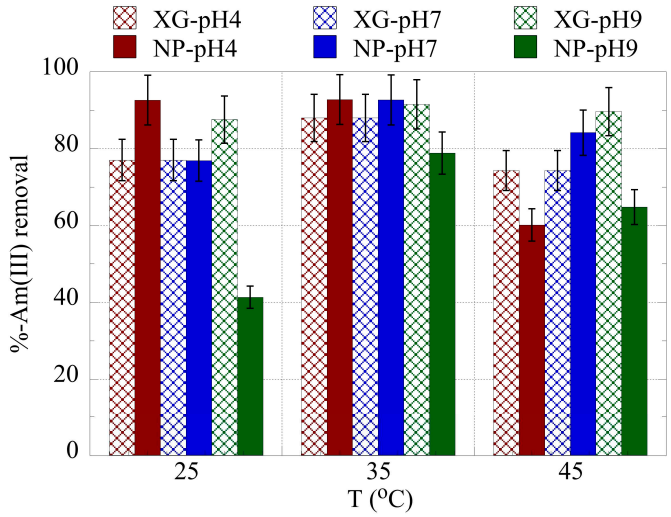

Figure 7. %-relative removal of Am(III) by nanoparticles (NP) and xerogels (XG) at ultra-trace levels at pH 4, 7, and 9, as a function of temperature. Experimental conditions: 10 mL of the solution, with 0.5 Bq/mL for both U-232 and Am-241 tracers, in different pH (pH = 4, 7, 9) and temperatures (25, 35, 45 ^{0}C).

The thermodynamic parameters ΔH^{o} and ΔS^{o} for the actinide ion adsorption by the xerogels and nanoparticles at pH 4, pH 7, and pH 9 have been evaluated using the linear form of the Van't Hoff formula and the associated data are graphically shown in Figures 8 and 9, respectively. According to the data in Figure 8 the ΔH^{o} values are positive suggesting an endothermic process. The lowest ΔH^{o} values for uranium are observed in the acidic pH area (pH 4) and the highest in the neutral pH area (pH 7) for the xerogels and in the alkaline area (pH 9) for the nanoparticles. For americium, the lowest ΔH^{o} values have been determined at pH 7 and pH 4, for the xerogels and the nanoparticles, respectively. On the other hand, the highest ΔH^{o} values for americium have been determined at pH 4 and pH 9 for the xerogels and the nanoparticles, respectively. Moreover, the nanoparticles present

Preprints (www.preprints.org) | NOT PEER-REVIEWED | Posted: 9 August 2023 doi:10.20944/preprints202308.0614.v1

significantly higher ΔH^o values for both radionuclides at pH 9. The latter is most probably associated with the formation of negatively charged species (e.g. $UO_2(CO_3)_3^{4-}$ and $Am(CO_3)_2^-$) in the alkaline pH range, which are extensively stabilized in solution. The endothermic character of the U(VI) surface binding at ultra-trace radionuclide levels has been also observed for the U(VI) binding by oxidized biochar fibers at pH 4 [76]. However, in the case of Am(III) binding by oxidized biochar fibers at pH 4 the adsorption process was exothermic and close to the values observed for the Am(III) adsorption by nanoparticles at pH 4.

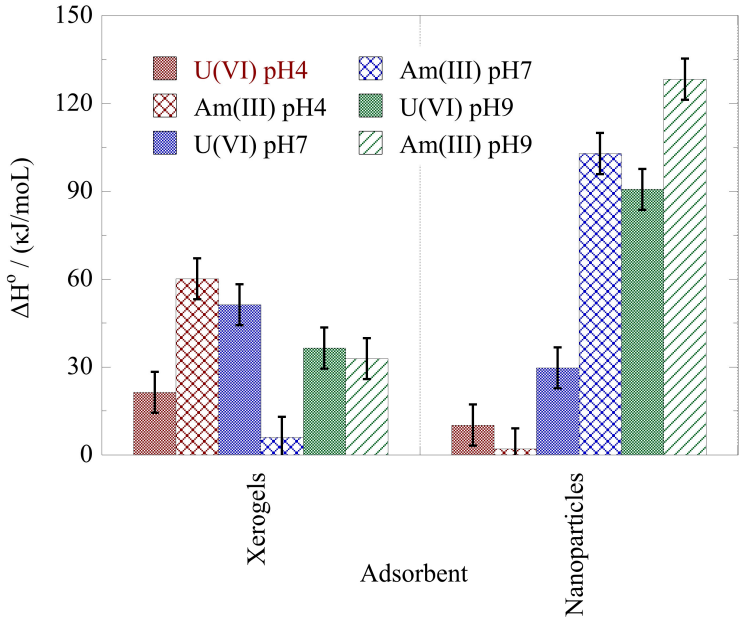

Figure 8. ΔH^o of the actinide ion adsorption by nanoparticles (NP) and xerogels (XG) at ultra-trace levels at pH 4, 7, and 9. Experimental conditions: 10 mL of the solution, with 0.5 Bq/mL for both U-232 and Am-241 tracers, at different temperatures (25, 35, 45 ^{0}C).

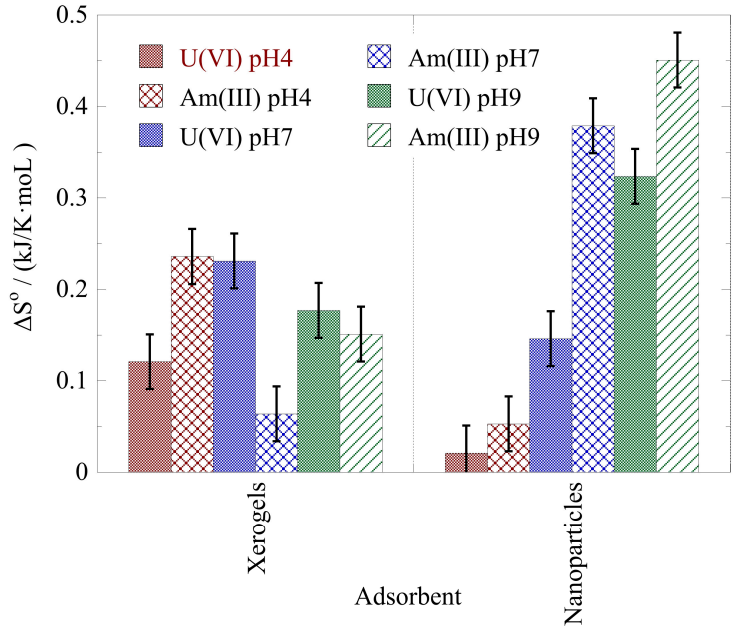

Figure 9. ΔS^o of the actinide ion adsorption by nanoparticles (NP) and xerogels (XG) at ultra-trace levels at pH 4, 7, and 9. Experimental conditions: 10 mL of the solution, with 0.5 Bq/mL for both U-232 and Am-241 tracers, at different temperatures (25, 35, 45 ^{0}C).

Preprints (www.preprints.org) | NOT PEER-REVIEWED | Posted: 9 August 2023 doi:10.20944/preprints202308.0614.v1

2.5. Radionuclide Interaction in Seawater

The removal efficiency of the americium and uranium radionuclides from seawater has been investigated after tracing seawater samples with americium-241 and uranium-232 and contacting them with the NP and XG adsorbents. The associated data are shown in Figure 10 and point out that in the case of XG, the adsorption efficiency for the two actinides is similar (~90%). On the other hand, the NP adsorbents present slightly higher adsorption efficiency for uranium (~80%) compared to americium (70%).

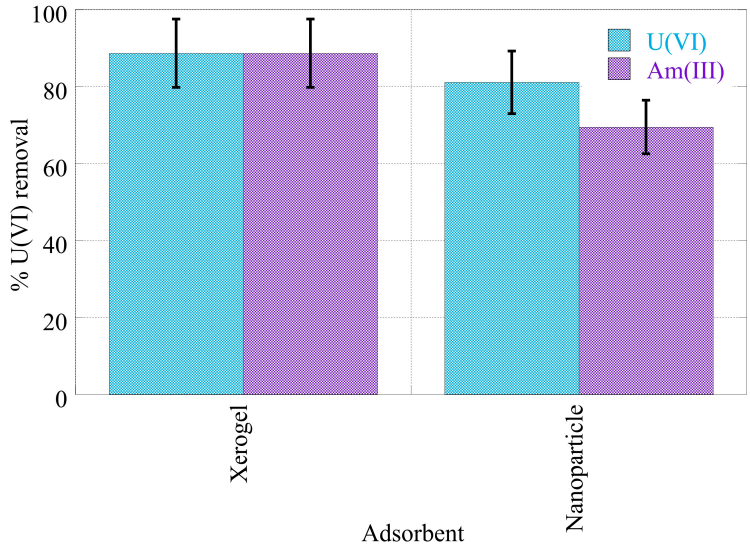

Figure 10. %-relative U(VI) and Am(III) removal by nanoparticles (NP) and xerogels (XG) at ultra-trace levels from seawater samples. Experimental conditions: 10 mL of the seawater solution, with 0.5 Bq/mL for both U-232 and Am-241 radionuclides.

The higher affinity of the adsorbents is depicted in Figure 11, that summarizes the K_d values of NP and XG for uranium and americium. According to the data in Figure 10, the chemical affinity of the adsorbents is significantly higher for uranium and the XG adsorbents possess higher affinity for both radionuclides compared to the NP adsorbents. This effect is similar to and has been observed also in laboratory/de-ionized water solutions. Nevertheless, despite the relatively low K_d values both materials present far higher removal efficiency of americium and uranium from seawater than oxidized biochar [77] or even X-alginate aerogels [7]. Xerogels could remove both actinide isotopes from seawater by almost 90%, whereas nanoparticles could remove uranium by 80% and americium by 70%. The above, along with their simple derivatization to increase the selectivity towards a specific radionuclide and their easy processing to be included in separation technologies, could make these materials very attractive for the treatment of radionuclide/actinide contaminated waters.

Preprints (www.preprints.org) | NOT PEER-REVIEWED | Posted: 9 August 2023 doi:10.20944/preprints202308.0614.v1

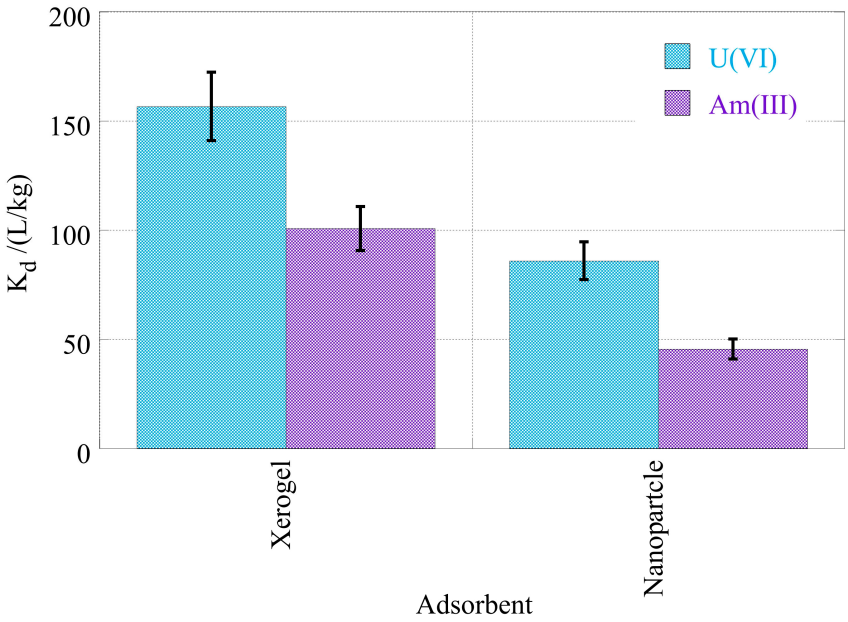

Figure 11. Adsorption efficiency ($\log_{10}K_d$) of U(VI) and Am(III) by Nanoparticles (NP) and Xerogels (XG) at ultra-trace levels from seawater samples. Experimental conditions: 10 mL of the seawater solution, with 0.5 Bq/mL for both U-232 and Am-241 radionuclides.

3. Conclusions

The conclusions that can be drawn from this study are the following:

- Hybrid silica-hyperbranched poly(ethylene imine) nanoparticles and xerogels present relatively high removal efficiency at pH 4 and pH 7 (> 70%) for Am(III) and U(VI).
- Generally, the adsorption process is relatively slow due to very low radionuclide concentrations and is governed by the actinide diffusion from the bulk solution to the composite surface.
- The actinide binding by the NP and XG composites is favored by increasing temperature indicating an endothermic and entropy-driven binding reaction.
- Compared to other adsorbents, which have been investigated regarding the removal of the studied actinide ions, both composites show far higher removal efficiency from laboratory and seawater samples, which is for xerogels almost 90% and for nanoparticles about 80% for uranium and 70% for americium.
- The simple derivatization of NP and XG to increase the selectivity towards specific actinides and other metal ions along with their easy implementation in water treatment technologies, could make these materials attractive candidates for the decontamination of actinide-contaminated waters, including seawaters.

4. Experimental section

4.1. Synthesis of the Composite Silica-PEI 750,000 Nanoparticles

A variation of the method proposed by Knecht et al. [79,80] for poly(amidoamine) PAMAM and poly(propylene imine) PPI dendrimers was employed for the preparation of the Silica-PEI nanocomposites as reported in our previous work [74]. In brief, a solution of hyperbranched PEI 750,000 (Mn = 750000 BASF, Ludwigshafen, Germany) solution 20 mM in primary and secondary amines was prepared by dissolving 0.29 g PEI 750,000 in 250 mL 20 mM phosphate buffer pH 7.5 (K_2HPO_4 Carlo Erba Reagenti, Rodano, Milano, Italy, KH_2PO_4 Merck Darmstadt Germany). 1 mL of this solution was added to 10 mL orthosilicic acid (1 M) prepared from the hydrolysis tetra ethoxy silane (Sigma-Aldrich, Steinheim, Germany) in 5 mM NNO_3 under vigorous stirring for 15 min. Silica precipitate was collected after centrifugation (10 min 12,000 × g) two washing with water and drying under vacuum over P_2O_5 (Sigma-Aldrich, Steinheim, Germany); yield 77%.

Preprints (www.preprints.org) | NOT PEER-REVIEWED | Posted: 9 August 2023 doi:10.20944/preprints202308.0614.v1

4.2. Synthesis of the Silica-PEI 750,000 Xerogels

This procedure is also described in detail in previous work [81]. Similar acid hydrolysis of a 1 M tetraethoxysilane solution (Sigma-Aldrich, Steinheim, Germany) with 25μL HNO_3 under stirring for 15 min produced 1 M orthosilicic acid. To 5 mL of this solution, 5 mL of PEI 750,000 (BASF, Ludwigshafen, Germany) aqueous solution (40 mM in primary and secondary amine groups) were added. The pH of the gel precursor solution was adjusted to 7.5 by adding K_2HPO_4 powder (Carlo Erba Reagenti, Rodano, Milano, Italy). Hydrogel formation was observed after about 1 to 2 hours and the reaction product was dried overnight over phosphorus pentoxide (Sigma-Aldrich, Steinheim, Germany) under vacuum to yield the silica-PEI 750,000 xerogel.

4.3. Adsorption Experiments

All adsorption experiments were conducted in 20 mL polyethylene vials under an ambient atmosphere and at various temperatures (25, 35, 45 ^oC). The test and reference solutions were prepared from the actinide standard solutions of uranium-232 (National Physical Laboratory, Teddington, UK) and americium-241 (North America Scientific Inc., Los Angeles, CA, USA) with radioactivity levels of 4.923 and 12.05 kBq/g, respectively. The composite adsorbents employed were based on dendritic poly(ethylene imine) 750,000: Silica-PEI 750,000 Nanoparticles (NP) and Silica-PEI 750,000 Xerogels (XG). The experiments were performed in de-ionized water solutions and the pH was adjusted to different values (pH 4, 7, and 9) using dilute aqueous solutions of NaOH and HCl, and seawater solution (SW). The seawater sample, which has been used in the present study was obtained from a local beach in Cyprus and the radioactive solutions prepared after the SW was filtered to remove any impurities. Radionuclides analysis was carried out using an alpha spectrometer (Canberra) by using stainless steel discs previously deposited with the two isotopes of U-232 and Am-241, as described elsewhere. [82].

The adsorption experiments were performed in 10 ml of a mixture of americium-241 and uranium-232 with an activity concentration of 0.5 mBq/mL for each radioisotope, which corresponds to molar concentration, [U-232] = $8.6x10^{-14}$ mol/L and [Am-241] = $8.17x10^{-13}$ mol/L. A small amount of 0.005 g for each material was added to the solution and the adsorption kinetics was studied for 10 days. The mixture in the flasks was stirred (45 min^{-1}) on a shaker (SK-R1807, DLAB). At specific time intervals, a 50 μl sample was taken from the test solutions and the actinide concentration was determined by means of alpha-spectroscopy. The alpha-spectrometer was previously calibrated by sample analysis using a standard reference source.

As the concentration of radionuclides is in the picomole range and the binding sites (B) of the composite surface are in large excess compared to the initial concentration of radionuclides, the partition coefficient, K_d adequately describes the equilibrium associated with the sorption of U -232 and Am-241:

$$K_d = C_{ads}/C_{aq}\ (L/Kg) \quad (1)$$

where C_{ads} (Bq/g) is the activity concentration of the actinide absorbed, and C_{aq} (Bq/L) is the concentration of the actinide in solution. The amount of U-232 and Am-241 adsorbed is calculated by subtracting the amount of actinides adsorbed on the walls of the polyethylene vial from the total amount of actinide adsorbed.

To calculate the standard enthalpy (ΔH^o) and entropy (ΔS^o) of the system, the following formula was used:

$$\ln K_d = \frac{-\Delta H^o}{RT} + \frac{\Delta S^o}{R} \quad (2)$$

The value of K_d is directly affected by both ΔH^o and ΔS^o and is inversely influenced by temperature. The slope of the relationship is determined by dividing the ΔH by the temperature (in Kelvin), multiplied by the gas constants (R). On the other hand, the intercept is determined by dividing the ΔS^o by the R.

The experiments were carried out in duplicate and the data evaluation was based on the mean values calculated from the results from the two different experiments. The relative uncertainty, which is basically determined by the measurement uncertainty, was estimated to be below 10%.

Author Contributions: Conceptualization, I.P., and M.A.; formal analysis, I.I., I.P., and M.A.; resources, I.P. and M.A.; writing—original draft preparation, I.I., M.A., and I.P.; writing—review and editing, I.I., I.P., and A.A..; funding acquisition, I.P., and M.A. All authors have read and agreed to the published version of the manuscript.

Funding: not applicable.

Acknowledgments: not applicable.

References

1. Choppin, G.R.; Jensen, M.P. Actinides in Solution: Complexation and Kinetics. In The Chemistry of the Actinide and Transactinide Elements; Morss, L.R., Edel-stein, N.M., Fuger, J., Eds.; Springer: Dordrecht, 2008; Chapter 23, pp. 285–345. https://doi.org/10.1007/1-4020-3598-5_23.
2. Seaborg, G.T. Uranium. In The Encyclopedia of the Chemical Elements; Reinhold Book Corporation: Skokie, Illinois, 1968; pp. 773–786.
3. Pashalidis, I.; Czerwinski, K.R.; Fanghänel, T.; Kim, J.I. Solid-Liquid Phase Equilibria of Pu(VI) and U(VI) in Aqueous Carbonate Systems. Determination of Stability Constants. *Radiochim. Acta* **1997**, *76*, 55–62. https://doi.org/10.1524/ract.1997.76.12.55.
4. Ioannidis, I.; Xenofontos, A.; Anastopoulos, I.; Pashalidis, I. Americium Sorption by Microplastics in Aqueous Solutions. *Coatings.* **2022**, *12*, 1452. https://doi.org/10.3390/coatings12101452.
5. Runde, W.; Meinrath, G.; Kim, J.I. A study of solid-liquid phase equilibria of trivalent lanthanide and actinide ions in carbonate systems. Radiochim. Acta 1992, 58–59, 93–100. https://doi.org/10.1524/ract.1992.5859.1.93.
6. Ioannidis, I.; Kinigopoulou, V.; Giannakoudakis, D.A.; Arkas, M.; Anastopoulos, I.; Triantafyllidis, K.S.; Pashalidis, I. Microplastics and disposable face masks as "Trojan Horse" for radionuclides pollution in water bodies–A review with emphasis on the involved interactions. *Sustainable Chemistry for the Environment.* **2023**, 100005. https://doi.org/10.1016/j.scenv.2023.100005.
7. Ioannidis, I.; Pashalidis, I.; Raptopoulos, G.; Paraskevopoulou, P. Radioactivity/Radionuclide (U-232 and Am-241) Removal from Waters by Polyurea-Crosslinked Alginate Aerogels in the Sub-Picomolar Concentration Range. *Gels.* **2023**, 9, 211. https://doi.org/10.3390/gels9030211.
8. Philippou, K.; Savva, I.; Pashalidis, I. Uranium(VI) Binding by Pine Needles Prior and after Chemical Modification. J. *Radioanal. Nucl. Chem.* **2018**, *318*, 2205–2211. https://doi.org/10.1007/s10967-018-6145-1.
9. Liatsou, I.; Michail, G.; Demetriou, M.; Pashalidis, I. Uranium Binding by Biochar Fibres Derived from Luffa Cylindrica after Controlled Surface Oxidation. *J. Radioanal. Nucl. Chem.* **2017**, *311*, 871–875. https://doi.org/10.1007/s10967-016-5063-3.
10. Hadjittofi, L.; Pashalidis, I. Uranium Sorption from Aqueous Solutions by Activated Biochar Fibres Investigated by FTIR Spectroscopy and Batch Experiments. *J. Radioanal. Nucl. Chem.* **2015**, *304*, 897–904. https://doi.org/10.1007/s10967-014-3868-5.
11. Stasi, C.; Georgiou, E.; Ioannidis, I.; Pashalidis, I. Uranium Removal from Laboratory and Environmental Waters by Oxidised Biochar Prepared from Palm Tree Fibres. *J. Radioanal. Nucl. Chem.* **2022**, *331*, 375–381. https://doi.org/10.1007/s10967-021-08076-1.
12. Bhalara, P.D.; Punetha, D.; Balasubramanian, K.A. Review of Potential Remediation Techniques for Uranium(VI) Ion Retrieval from Contaminated Aqueous Environment. *J. Environ. Chem. Eng.* **2014**, *2*, 1621–1634. https://doi.org/10.1016/j.jece.2014.06.007.
13. Ioannidis, I.; Anastopoulos, I.; Giannakopoulos, K.; Arkas, M.; Dosche, C.; Pashalidis, I. A comprehensive investigation on the sorption of U (VI) and Eu (III) by polyamide microplastics: Surface-assisted microparticle formation. *J. Mol. Liquids* **2022**, *368*, 120757. https://doi.org/10.1016/j.molliq.2022.120757.
14. Yin, J.; Yang, S.; He, W.; Zhao, T.; Li, C.; Hua, D. Biogene-Derived Aerogels for Simultaneously Selective Adsorption of Uranium(VI) and Strontium(II) by Co-Imprinting Method. *Sep. Purif. Technol.* **2021**, *271*, 118849. https://doi.org/10.1016/j.seppur.2021.118849.
15. Anastopoulos, I.; Milojković, J.V.; Tsigkou, K.; Zafiri, C.; Lopičić, Z.R.; Kornaros, M.; Pashalidis, I. A Nappies Management By-Product for the Treatment of Uranium-Contaminated Waters. *J. Hazard. Mater.* **2021**, *404*, 124147. https://doi.org/10.1016/j.jhazmat.2020.124147.
16. Liatsou, I.; Savva, I.; Vasile, E.; Vekas, L.; Marinica, O.; Mpekris, F.; Pashalidis, I.; Krasia-Christoforou, T. Magnetoresponsive Polymer Networks as Adsorbents for the Removal of U(VI) Ions from Aqueous Media. *Eur. Polym. J.* **2017**, *97*, 138–146. https://doi.org/10.1016/j.eurpolymj.2017.10.005.

17. Paschalidou, P.; Liatsou, I.; Pashalidis, I.; et al. Effect of surface and textural characteristics on uranium adsorption by nanoporous titania. *J. Radioanal. Nucl. Chem.* **2017**, *314*, 1141–1147. https://doi.org/10.1007/s10967-017-5475-8.
18. Konstantinou, M.; Demetriou, A.; Pashalidis, I. Adsorption of hexavalent uranium on dunite. *Global NEST* Journal **2007**, *9*(3), 229–236. https://doi.org/10.30955/gnj.000446. .
19. Guo, H.; Mei, P.; Xiao, J.; Huang, X.; Ishag, A.; Sun, Y. Carbon Materials for Extraction of Uranium from Seawater. *Chemosphere* **2021**, *278*, 130411. https://doi.org/10.1016/j.chemosphere.2021.130411.
20. Panagiotou, N.; Liatsou, I.; Pournara, A.; Angeli, G.K.; Giappa, R.M.; Tylianakis, E.; Manos, M.J.; Froudakis, G.E.; Trikalitis, P.N.; Pashalidis, I.; et al. Water-Stable 2-D Zr MOFs with Exceptional UO22+ Sorption Capability. *J. Mater. Chem. A.* **2020**, *8*, 1849–1857. https://doi.org/10.1039/C9TA10701K.
21. Liu, H.; Fu, T.; Mao, Y. Metal–Organic Framework-Based Materials for Adsorption and Detection of Uranium(VI) from Aqueous Solution. *ACS Omega* **2022**, *7*, 14430–14456. https://doi.org/10.1021/acsomega.2c00597.
22. Koppula, S.; Manabolu Surya, S.; Katari, N.K.; Dhami, P.S.; Sivasankaran Nair, R.K. Mesoporous MOF Composite for Efficient Removal of Uranium, Methyl Orange, Methylene Blue, and Congo Red Dyes from Aqueous Solutions. *Appl. Organomet. Chem*. **2022**, *36*, e6554. https://doi.org/10.1002/aoc.6554.
23. Li, N.; Yang, L.; Wang, D.; Tang, C.; Deng, W.; Wang, Z. High-Capacity Amidoxime-Functionalized β-Cyclodextrin/Graphene Aerogel for Selective Uranium Capture. *Environ. Sci. Technol.* **2021**, *55*, 9181–9188.
24. Liu, W.; Zhang, L.; Chen, F.; Wang, H.; Wang, Q.; Liang, K. Efficiency and Mechanism of Adsorption of Low-Concentration Uranium from Water by a New Chitosan/Aluminum Sludge Composite Aerogel. *Dalton Trans.* **2020**, *49*, 3209–3221.
25. Georgiou, E.; Raptopoulos, G.; Papastergiou, M.; Paraskevopoulou, P.; Pashalidis, I. Extremely Efficient Uranium Removal from Aqueous Environments with Polyurea-Cross-Linked Alginate Aerogel Beads. *ACS Applied Polymer Materials.* **2022**, *4*(2), 920-928. https://doi.org/10.1021/acsapm.1c01400.
26. Georgiou, E.; Raptopoulos, G.; Anastopoulos, I.; Giannakoudakis, D.A.; Arkas, M.; Paraskevopoulou, P.; Pashalidis, I. Uranium Removal from Aqueous Solutions by Aerogel-Based Adsorbents-*A Critical Review. Nanomaterials*. **2023**, *13*, 363. https://doi.org/10.3390/nano13020363.
27. Ioannou, K.; Hadjiyiannis, P.; Liatsou, I.; Pashalidis, I. U(VI) Adsorption by Biochar Fiber-MnO_2 Composites. *J. Radioanal. Nucl. Chem*. **2019**, *320*, 425-432. https://doi.org/10.1007/s10967-019-06479-9.
28. Philippou, K.; Anastopoulos, I.; Dosche, C.; Pashalidis, I. Synthesis and Characterization of a Novel Fe_3O_4-Loaded Oxidized Biochar from Pine Needles and Its Application for Uranium Removal. Kinetic, Thermodynamic, and Mechanistic Analysis. *J. Environ. Manag.* **2019**, *252*, 109677. https://doi.org/10.1016/j.jenvman.2019.109677.
29. Philippou, K.; Christou, C.N.; Socoliuc, V.; Vekas, L.; TanasPÉ, E.; Miclau, M.; Pashalidis, I.; Krasia-Christoforou, T. Superparamagnetic Polyvinylpyrrolidone/Chitosan/Fe_3O_4 Electrospun Nanofibers as Effective U(VI) Adsorbents. *J. Appl. Polym. Sci.* **2021**, *138*, 50212. https://doi.org/10.1002/app.50212.
30. Guo, D.; Song, X.; Zhang, L.; Chen, W.; Chu, D.; Tan, L. Recovery of Uranium (VI) from Aqueous Solutions by the Polyethyleneimine-Functionalized Reduced Graphene Oxide/Molybdenum Disulfide Composition Aerogels. *J. Taiwan Inst. Chem. Eng.* **2020**, *106*, 198–205. https://doi.org/10.1016/j.jtice.2019.09.029.
31. Huang, Z.; Li, Z.; Zheng, L.; Zhou, L.; Chai, Z.; Wang, X.; Shi, W. Interaction Mechanism of Uranium(VI) with Three-Dimensional Graphene Oxide-Chitosan Composite: Insights from Batch Experiments, IR, XPS, and EXAFS Spectroscopy. *Chem. Eng. J.* **2017**, *328*, 1066–1074. https://doi.org/10.1016/j.cej.2017.07.067.
32. Buhleier, E.; Wehner, W.; Vogtle, F. "Cascade"- and "nonskid-chain-like" syntheses of molecular cavity topologies. *Synthesis.* **1978**, 155–158. https://doi.org/10.1055/s-1978-24702.
33. de Gennes, P.G.; Hervet, H. Statistics of "starburst" polymers. *J. Phys. Lett.* **1983**, *44*, 351–360. https://doi.org/10.1051/jphyslet:01983004409035100.
34. Tomalia, D.A.; Fréchet, J.M. Discovery of dendrimers and dendritic polymers: A brief historical perspective. *J. Polym. Sci. Part A: Polym. Chem*. **2002**, *40*, 2719–2728. https://doi.org/10.1002/pola.10301
35. Douloudi, M.; Nikoli, E.; Katsika, T.; Arkas, M. Dendritic polymers for water resources remediation. *In Novel Materials for Environmental Remediation Applications; Elsevier:* **2023**; pp. 435-490. https://doi.org/10.1016/C2021-0-00209-1.
36. Arkas, M.; Tsiourvas, D.; Paleos, C.M. Functional dendritic polymers for the development of hybrid materials for water purification. *Macromol. Mater. Eng.* **2010**, *295*(10), 883-898. https://doi.org/10.1002/mame.201000219.
37. Vöegtle, F.; Gestermann, S.; Hesse, R.; Schwierz, H.; Windisch, B. Functional dendrimers. *Prog. Polym. Sci.* **2000**, *25*, 987-1041. https://doi.org/10.1016/S0079-6700(00)00017-4
38. Caminade, A.M.; Turrin, C.O.; Laurent, R.; Ouali, A.; Delavaux-Nicot, B. (Eds.) Dendrimers: Towards Catalytic, Material, and Biomedical Uses; John Wiley & Sons: Hoboken, NJ, USA, 2011.
39. Arkas, M.; Eleades, L.; Paleos, C.M.; Tsiourvas, D. Alkylated hyperbranched polymers as molecular nanosponges for the purification of water from polycyclic aromatic hydrocarbons. *J. Appl. Polym. Sci.* **2005**, *97*(6), 2299-2305. https://doi.org/10.1002/app.22026.

40. Arkas, M.; Anastopoulos, I.; Giannakoudakis, D.A.; Pashalidis, I.; Katsika, T.; Nikoli, E.; Panagiotopoulos, R.; Fotopoulou, A.; Vardavoulias, M.; Douloudi, M. Catalytic Neutralization of water pollutants mediated by dendritic polymers. *Nanomaterials* **2022**, *12*(3), 445. https://doi.org/10.3390/nano12030445.
41. Arkas, M.; Panagiotaki, K.; Kitsou, I.; Petrakli, F. Dendritic Polymer—Enhanced Ultrafiltration. *In Nanoscale Materials in Water Purification; Elsevier*: **2019**; pp. 111-152. https://doi.org/10.1016/B978-0-12-813926-4.00010-0.
42. Ilaiyaraja, P.; Deb, A.S.; Ponraju, D.; Ali, S.M.; Venkatraman, B. Surface Engineering of PA-MAM-SDB Chelating Resin with Diglycolamic Acid (DGA) Functional Group for Efficient Sorption of U(VI) and Th(IV) from Aqueous Medium. *J. Hazard. Mater*. **2017**, *328*, 1-11. https://doi.org/10.1016/j.jhazmat.2017.01.001.
43. Ilaiyaraja, P.; Deb, A.K.S.; Sivasubramanian, K.; Ponraju, D.; Venkatraman, B. Adsorption of Uranium from Aqueous Solution by PAMAM Dendron Functionalized Styrene Divinylbenzene. **J. Hazard. Mater. 2013**, *250*, 155-166. https://doi.org/10.1016/j.jhazmat.2013.01.040.
44. Ilaiyaraja, P.; Deb, A.K.S.; Ponraju, D.; Venkatraman, B. Xanthate Functionalized PAMAM Dendrimer (XFPD) Chelating Ligand for Treatment of Radioactive Liquid Wastes. *J. Environ. Chem. Eng.* **2015**, *3*(2), 1047-1054. https://doi.org/10.1016/j.jece.2015.03.013.
45. Priyadarshini, N.; Ilaiyaraja, P. Adsorption of U(VI) and Th(IV) from Simulated Nuclear Waste Using PAMAM and DGA Functionalized PAMAM Dendron Grafted Styrene Divinylbenzene Chelating Resins. *Chem. Pap.* **2019**, *73*(11), 2879-2884. https://doi.org/10.1007/s11696-019-00830-w.
46. Ardoin, N.; Astruc, D. Molecular trees: From syntheses towards applications. Bull. Soc. Chim. Fr. **1995**, *9*, 875–909.
47. Bosman, D.A.; Janssen, H.M.; Meijer, E.W. About dendrimers: Structure, physical properties, applications. Chem. Rev. **1999**, *99*, 1665–1688. https://doi.org/10.1021/cr970069y.
48. Dvornic, P.R.; Tomalia, D.A. November. Starburst® Dendrimers: A Conceptual Approach to Nanoscopic Chemistry and Architecture. *In Macromolecular Symposia; Springer: Heidelberg/Berlin, Germany*, **1994**,*88*, 123–148. https://doi.org/10.1002/masy.19940880111.
49. Tully, D.C.; Fréchet, J.M. Dendrimers at Surfaces and Interfaces: Chemistry and Applications. *Chem. Commun.* **2001**, *14*, 1229–1239. https://doi.org/10.1039/B104290B.
50. Zeng, F.; Zimmerman, S.C. Dendrimers in Supramolecular Chemistry: From Molecular Recognition to Self-Assembly. *Chem. Rev.* **1997**, *97*, 1681–1712. https://doi.org/10.1021/cr9603892.
51. Jikei, M.; Kakimoto, M.A. Hyperbranched Polymers: A Promising New Class of Materials. *Prog. Polym. Sci.* **2001**, *26*, 1233–1285. https://doi.org/10.1016/S0079-6700(01)00018-1.
52. Kim, Y.H. Hyperbranched Polymers 10 Years After. *J. Polym. Sci. Part A Polym. Chem.* **1998**, *36*, 1685–1698. https://doi.org/10.1002/(SICI)1099-0518.
53. Malmström, E.; Hult, A. Hyperbranched Polymers. *J. Macromol. Sci. Part C Polym. Rev*. **1997**, *37*, 555–579. https://doi.org/10.1080/15321799708018375.
54. Sunder, A.; Heinemann, J.; Frey, H. Controlling the Growth of Polymer Trees: Concepts and Perspectives for Hyperbranched Polymers. *Chem. A Eur. J.* **2000**, *6*, 2499–2506. https://doi.org/10.1002/1521-3765(20000717)6:14.
55. Voit, B.I. Hyperbranched Polymers: A Chance and a Challenge. *Comptes Rendus Chim.* **2003**, *6*, 821–832.
56. Yates, C.R.; Hayes, W. Synthesis and Applications of Hyperbranched Polymers. Eur. Polym. J. **2004**, *40*, 1257–1281. https://doi.org/10.1016/j.eurpolymj.2004.02.007.
57. Zheng, Y.; Li, S.; Weng, Z.; Gao, C. Hyperbranched Polymers: Advances from Synthesis to Applications. *Chem. Soc. Rev.* **2015**, *44*, 4091–4130.
58. Li, H.; Sun, J.; Zhu, H.; Wu, H.; Zhang, H.; Gu, Z.; Luo, K. Recent Advances in Development of Dendritic Polymer-Based Nanomedicines for Cancer Diagnosis. *Wiley Interdiscip. Rev. Nanomed. Nanobiotechnol*. **2021**, *13*, 1670. https://doi.org/10.1002/wnan.1670.
59. Ma, Y.; Mou, Q.; Wang, D.; Zhu, X.; Yan, D. Dendritic Polymers for Theranostics. Theranostics **2016**, *6*, 930. https://doi.org/10.7150/thno.14855.
60. Korake, S.; Shaikh, A.; Salve, R.; Gajbhiye, K.R.; Gajbhiye, V.; Pawar, A. Biodegradable Dendritic Boltorn™ Nano-constructs: A Promising Avenue for Cancer Theranostics. *Int. J. Pharm.* **2021**, *594*, 120177. https://doi.org/10.1016/j.ijpharm.2020.120177.
61. German, N.; Popov, A.; Ramanavicius, A.; Ramanaviciene, A. Development and Practical Application of Glucose Biosensor Based on Dendritic Gold Nanostructures Modified by Conducting Polymers. *Biosensors* **2022**, *12*, 641. https://doi: 10.3390/bios12080641.
62. Jimenez, A.; Armada, M.P.G.; Losada, J.; Villena, C.; Alonso, B.; Casado, C.M. Amperometric Biosensors for NADH Based on Hyperbranched Dendritic Ferrocene Polymers and Pt Nanoparticles. *Sens. Actuators B Chem.* **2014**, *190*, 111–119. https://doi.org/10.1016/j.snb.2013.08.072.
63. Arkas, M.; Kythreoti, G.; Favvas, E.P.; Giannakopoulos, K.; Mouti, N.; Arvanitopoulou, M.; Athanasiou, A.; Douloudi, M.; Nikoli, E.Vardavoulias, M.; et al. Hydrophilic Antimicrobial Coatings for Medical Leathers from Silica-Dendritic Polymer-Silver Nanoparticle Composite Xerogels. *Textiles* **2022**, *2*, 464–485. https://doi.org/10.3390/textiles2030026.

64. Marcos, M.; Martín-Rapún, R.; Omenat, A.; Serrano, J.L. Highly Congested Liquid Crystal Structures: Dendrimers, Dendrons, Dendronized and Hyperbranched Polymers. *Chem. Soc. Rev.* **2007**, *36*, 1889–1901. https://doi.org/10.1039/B611123H.
65. Tsiourvas, D.; Arkas, M. Columnar and Smectic Self-Assembly Deriving from Non-Ionic Amphiphilic Hyperbranched Polyethylene Imine Polymers and Induced by Hydrogen Bonding and Segregation into Polar and Non-Polar Parts. *Polymer* **2013**, *54*, 1114–1122. https://doi.org/10.1016/j.polymer.2012.12.023.
66. Arkas, M.; Kitsou, I.; Gkouma, A.; Papageorgiou, M. The Role of Hydrogen Bonds in the Mesomorphic Behaviour of Supramolecular Assemblies Organized in Dendritic Architectures. *Liq. Cryst.* Rev. **2019**, *7*, 60–105.
67. Paleos, C.M.; Tsiourvas, D.; Sideratou, Z.; Tziveleka, L.A. Drug Delivery Using Multifunctional Dendrimers and Hyperbranched Polymers. *Expert Opin. Drug Deliv.* **2010**, *7*, 1387–1398. https://doi:10.1517/17425247.2010.534981.
68. Douloudi, M.; Nikoli, E.; Katsika, T.; Vardavoulias, M.; Arkas, M. Dendritic Polymers as Promising Additives for the Manufacturing of Hybrid Organoceramic Nanocomposites with Ameliorated Properties Suitable for an Extensive Diversity of Applications. Nanomaterials **2020**, *11*, 19. https://doi:10.3390/nano11010019.
69. Tsetsekou, A., Arkas, M., Kritikaki, A., Simonetis, S. and Tsiourvas, D., 2008. Optimization of Hybrid Hyperbranched Polymer/Ceramic Filters for the Efficient Absorption of Polyaromatic Hydrocarbons from Water. *Journal of Membrane Science*, *311*(1-2), pp.128-135. https://doi.org/10.1016/j.memsci.2007.12.017.
70. Pang, Y.; Zeng, G.; Tang, L.; Zhang, Y.; Liu, Y.; Lei, X.; Li, Z.; Zhang, J.; Xie, G. PEI-Grafted Magnetic Porous Powder for Highly Effective Adsorption of Heavy Metal Ions. *Desalination* **2011**, *281*, 278–284. https://doi.org/10.1016/j.desal.2011.08.001.
71. Arkas, M.; Tsiourvas, D.; Paleos, C.M. Organosilicon Dendritic Networks in Porous Ceramics for Water Purification. *Chem. Mater*. **2005**, *17*, 3439–3444. https://doi.org/10.1021/cm047981p.
72. Allabashi, R.; Arkas, M.; Hörmann, G.; Tsiourvas, D. Removal of Some Organic Pollutants in Water Employing Ceramic Membranes Impregnated with Cross-Linked Silylated Dendritic and Cyclodextrin Polymers. *Water Research.* **2007**, *41*(2) 476-486. https://doi.org/10.1016/j.watres.2006.10.011.
73. Kroger, N.; Deutzmann, R.; Sumper, M. Polycationic Peptides from Diatom Biosilica that Direct Silica Nanosphere Formation. *Science.* **1999**, *286*, 1129–1132. https://doi.org/10.1126/science.286.5442.112.
74. Arkas, M.; Tsiourvas, D. Organic/Inorganic Hybrid Nanospheres Based on Hyperbranched Poly(ethylene imine) Encapsulated into Silica for the Sorption of Toxic Metal Ions and Polycyclic Aromatic Hydrocarbons from Water. *J. Hazard. Mater.* **2009**, *170*, 35–42. https://doi.org/10.1016/j.jhazmat.2009.05.031.
75. Arkas, M.; Giannakopoulos, K.; Favvas, E.P.; Papageorgiou, S.; Theodorakopoulos, G.V.; Giannoulatou, A.; Vardavoulias, M.; Giannakoudakis, D.A.; Triantafyllidis, K.S.; Georgiou, E.; et al. Comparative Study of the U(VI) Adsorption by Hybrid Silica-Hyperbranched Poly(ethylene imine) Nanoparticles and Xerogels. *Nanomaterials* **2023**, *13*, 1794. https://doi.org/10.3390/nano13111794.
76. Philippou, M.; Pashalidis, I.; Theocharis, C.R. Uranium Isotope (U-232) Removal from Waters by Biochar Fibers: An Adsorption Study in the Sub-Picomolar Concentration Range. *Molecules* **2022**, *27*, 6765. https://doi.org/10.3390/molecules27196765.
77. Philippou, M.; Pashalidis, I.; Kalderis, D. Removal of 241Am from Aqueous Solutions by Adsorption on Sponge Gourd Biochar. *Molecules* **2023**, *28*, 2552. https://doi.org/10.3390/molecules28062552.
78. Konstantinou, M.; Pashalidis, I. Speciation and Spectrophotometric Determination of Uranium in Seawater. *Mediterr. Mar. Sci*. **2004**, *5*, 55–60. https://doi:10.12681/mms.210.
79. Knecht, M.R.; Wright, D.W. Amine-Terminated Dendrimers as Biomimetic Templates for Silica Nanosphere Formation. Langmuir **2004**, *20*, 4728–4732.
80. Knecht, M.R.; Sewell, S.L.; Wright, D.W. Size Control of Dendrimer-Templated Silica. Langmuir **2005**, *21*, 2058–2061. https://doi.org/10.1021/la0494019.
81. Jensen, L.K.; Jensen, H.E.; Blirup-Plum, S.A.; Bue, M.; Hanberg, P.; Kvich, L.; Aalbæk, B.; López, Y.; Soto, S.M.; Douloudi, M.; Papageorgiou, M. Coating of Bone Implants with Silica, Hyperbranched Poly(ethyleneimine), and Gentamicin Prevents Development of Osteomyelitis in a Porcine Model. *Materialia* **2022**, *24*, 101473. https://doi.org/10.1016/j.mtla.2022.101473.
82. Kiliari, T.; Pashalidis, I. Simplified Alpha-Spectroscopic Analysis of Uranium in Natural Waters after Its Separation by Cation-Exchange. *Radiat. Meas.* **2010**, *45*, 966–968. https://doi.org/10.1016/j.radmeas.2010.06.024.